Mass Transfer Effects in Polycondensation Reactors Wherein Functional Groups Are Not Equally Reactive

SANTOSH K. GUPTA,* N. L. AGARWALLA, and ANIL KUMAR,
Department of Chemical Engineering, Indian Institute of Technology, Kanpur-208016, India

Synopsis

Three simplified models of polycondensation reactors are considered in which the condensation product is continuously removed by application of vacuum. Reversible polycondensation reactions of monomers violating the equal reactivity hypothesis have been simulated in these reactors. The effect of various rate and reactor design variables on the molecular weight distribution (MWD) and its moments is studied. It is observed that when the reverse reactions are rapid, the results are fairly sensitive to the level of vacuum applied and to the mass transfer resistance; whereas when the forward reactions predominate, results lie very close to earlier plots for the corresponding irreversible polymerizations. These reactor variables then have relatively small influence on the MWD. Splitting of the MWD curves for odd and even values of n is observed under certain conditions, the effects being more pronounced in the presence of mass transfer than in its absence.

Introduction

Simulations of irreversible polycondensation reactions wherein the functional groups are equally reactive[1-3] have been carried out for batch reactors,[1-5] ideal continuous-flow, stirred-tank reactors (HCSTR),[6-8] and continuous-flow stirred-tank reactors with segregation (SCSTR).[9] In many practical polymerizations, the equal reactivity hypothesis is violated, and examples of these have been compiled recently.[2,10] Several kinetic schemes have been proposed by various workers[11-16] modeling real polymerizations and these have been simulated for commonly used reactors, viz., batch reactors,[11-16] HCSTRs[17-19] and SCSTRs.[20] Unfortunately, all these studies assume irreversibility of the various condensation reactions, and so, at best, these studies approximate the actual course of polycondensations in industry during the initial stages only. In practical situations, the polycondensation reactions are reversible, and usually a vacuum is applied to the reaction mass in order to drive the reactions in the forward direction to give high-molecular-weight products.

Reversible polycondensations with equal reactivity of functional groups have been studied by Abraham[21] and Mellichamp,[22] and similar work on reversible polycondensations violating the equal reactivity hypothesis has been reported by Gupta et al.[10,23] recently. In these studies it has been assumed that the condensation product is not removed during the polymerization. Secor,[24] Hoftyzer and Van Krevelen,[25] and Amon and Denson[26] studied the progress of polymerization at different locations of the reaction mass when a vacuum is applied to remove the condensation product.

In the present paper, Secor's work on reversible polycondensations obeying

* To whom correspondence should be addressed.

Journal of Applied Polymer Science, Vol. 27, 1217–1231 (1982)
 CCC 0021-8995/82/041217-15$02.50

the equal reactivity hypothesis, with the condensation product diffusing toward the vacuum side, is extended to the case of reversible polycondensations violating this hypothesis. Three types of reactor geometries commonly encountered in industrial practice are investigated. Based on results derived from this relatively fundamental study, one can draw qualitative conclusions for more complex polymerizations under similar reactor conditions.[27–31]

FORMULATION

Reversible condensation polymerizations of the AB type bifunctional molecules can be represented in general as

$$\begin{aligned}
&P_n + P_m \xrightarrow{k_{p,mn}} P_{n+m} + W \qquad m, n = 1, 2, \ldots \\
&P_1 + P_{n-1} \xleftarrow{k'_{p\,n,1}} P_n + W \qquad n = 2, 3 \ldots \\
&P_2 + P_{n-2} \xleftarrow{k'_{p\,n2}} \\
&\quad\vdots \\
&2P_{n/2} \xleftarrow{n \text{ even } k'_{p,n,(n)/2}} \\
&P_{n-1/2} + P_{n+1/2} \xleftarrow{n \text{ odd } k'_{p,n,(n-1)/2}}
\end{aligned} \tag{1}$$

where P_m represents a bifunctional molecule having m repeat units and W is the condensation product. In one of the kinetic schemes, it is assumed that the forward rate constant between a monomer and a monomer is different from that between any two other species[12,17]:

$$\begin{aligned}
k_{p,11} &= 2(k_{11}/2) \\
k_{p,mn} &= 2(k_p);\ m \neq n;\ m, n = 1, 2, 3, \ldots \\
&= 2(k_p/2);\ m = n;\ m, n > 1
\end{aligned} \tag{2}$$

where the factor of $\frac{1}{2}$ in paranthesis for $m = n$ is required to prevent counting of molecular collisions twice,[3] and the factor of 2 outside the parantheses is required to account for the fact that either functional group A on P_n can react with B on P_m or B on P_n can react with A on P_m. In modeling the reverse rate constants, it has been assumed that the rate of reaction between W and a reacted —AB— group at the ends of P_n is different from that between W and an —AB—

group in the "interior" of P_n:

$$\left.\begin{aligned} k'_{p,21} &= k'_e \\ k'_{p,n1} &= 2k'_e \\ k'_{p,ni} &= 2k'_p; \quad i = 2, 3, \ldots \frac{n}{2} \text{ (for even } n) \\ & \qquad\quad i = 2, 3, \ldots \frac{n-1}{2} \text{ (for odd } n) \end{aligned}\right\} \quad n = 3, 4, \ldots \qquad (3)$$

Again, a factor of 2 is required to account for the fact that there are two identical —AB— groups of P_n i units away from either of its two ends. k_{11}, k_p, k'_e, and k'_p thus represent the functional group reactivities and are similar to the rate constants used by Flory.[1]

The above kinetic scheme (called Model I) is a good representation of actual polymerizations in some cases. For other systems, it represents one of two limiting extremes—the other limiting model (called Model II) is presented in Ref. 23. One important advantage of this kinetic scheme is that it is probably the simplest theoretical model which brings out the major features of polymerizations where the equal reactivity hypothesis is violated.

In commercial polycondensation reactors, the reactions are driven in the forward direction by application of high vacuums. The condensation product W diffuses through the reaction mass to the surface at which vacuum is applied and is continuously removed. In one common reactor (wiped-film type), polymerization occurs in a thin film inside a cylindrical tank as shown in Figure 1(a), and a vacuum is applied inside. Since the film is thin, the effect of curvature is small and the film may be modeled as shown in Figure 1(b), where the cylindrical reaction mass is replaced by an infinite slab of thickness L.

A pool-type reactor is another possibility in which an inert gas is bubbled through, as in Figure 1(c) (or the condensation product may itself vaporize, forming gas bubbles which move towards the surface). In general, the gas bubbles will be of all sizes and will be randomly distributed. However, a simple model of such a reactor would be to assume equal-sized, spherical gas bubbles distributed uniformly. One can then associate with each bubble of radius R_1 a hollow spherical shell of the reaction mass extending over $R_1 \leqslant r \leqslant R_2$ [Fig. 1(d)] with the condensation product diffusing toward the hollow space, where its concentration is lower. At $r = R_2$, the outer surface of this hollow sphere, conditions are symmetrical on either side.

The third system is a pool of polymerizing material with an extremely rapid vaporization of W. In such situations, the reacting mass is no more continuous but gets isolated into several small regions separated by the vaporized W, as shown in Figure 1(e). A simple model of this situation would be to consider each reacting zone as a sphere of radius R_2, with diffusion of W from its interior to the surface $r = R_2$.

In this study, these three idealized models of common polymerization reactors are considered, and molecular weight distributions (MWDs) are obtained using the kinetic scheme presented above, in which the equal reactivity hypothesis is violated. In the earlier work of Secor,[24] only the models shown in Figures 1(b) and 1(f) were considered and the number-average chain length *alone* was obtained for the equal reactivity case.

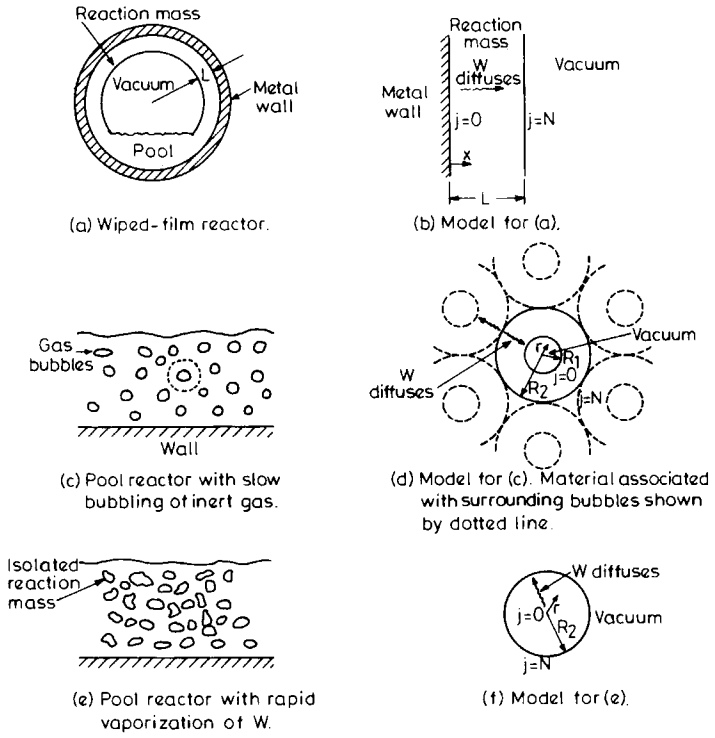

Fig. 1. Three common types of reactors and their simplified models.

Mass balance equations for the several models of the polymerization reactor shown in Figure 1, using the kinetic scheme given in eqs. (1)–(3), are written as[32]

$$\frac{\partial[P_1]}{\partial t} = -2(k_{11} - k_p)\,[P_1]^2 - 2k_p[P_1][P] + 2k_e'[W] \sum_{n=2}^{\infty} [P_n] \qquad (a)$$

$$\frac{\partial[P_2]}{\partial t} = -2k_p[P_2][P] + k_{11}[P_1]^2 + 2k_e'\,[P_3][W] + 2k_p'\,[W] \sum_{n=4}^{\infty} [P_n] - k_e'\,[P_2][W] \qquad (b)$$

$$\frac{\partial[P_n]}{\partial t} = k_p \sum_{m=1}^{n-1} [P_m][P_{n-m}] - 2k_p[P_n][P] + 2k_e'\,[P_{n+1}][W] + 2k_p'\,[W] \sum_{m=n+2}^{\infty} [P_m] - 2k_e'\,[P_n][W] - k_p'(n-3)\,[P_n][W] \qquad n = 3, 4 \ldots \qquad (c)$$

$$\frac{\partial[W]}{\partial t} = D_w \left\{ \frac{\partial^2[W]}{\partial \zeta^2} + \frac{\lambda}{\zeta} \frac{\partial[W]}{\partial \zeta} \right\} + k_{11}[P_1]^2 + k_p \sum_{n=3}^{\infty} \sum_{m=1}^{n-1} [P_m][P_{n-m}] - k_e'\,[P_2][W] - \sum_{n=3}^{\infty} \{2k_e' + (n-3)k_p'\}\,[W][P_n] \qquad (4)$$

where [ ] represent the molar concentration of any species, D_w is the diffusivity of the condensation product, and [P] is the sum of the concentrations of the in-

dividual mers, $P_1, P_2, \ldots$ In eq. (4), $\zeta = x$, $\lambda = 0$ is to be used for the film [Fig. 1(b)] and $\zeta = r$, $\lambda = 2$ for the solid [Fig. 1(d)] and hollow [Fig. 1(f)] sphere models of the reactor. The assumptions used in obtaining eq. (4) are similar to those used earlier by Secor[24] and by Amon and Denson.[26]

The following initial and boundary conditions are used:

Initial condition (pure monomer), $t = 0$:

$$\left.\begin{array}{l} \text{(i) } [P_1] = [P] = [P_1]_0 \\ \text{(ii) } [P_2] = [P_3] = \ldots = [W] = 0 \end{array}\right\} \begin{array}{l} 0 \le x \le L \text{ (film)} \\ 0 \le r \le R_2 \text{ (solid sphere)} \\ R_1 \le r \le R_2 \text{ (hollow sphere)} \end{array} \qquad \text{(a)}$$

Boundary condition, $t > 0$:

(i) $[W] = [W]_s$ at $x = L$ (film), $r = R_2$ (solid sphere) or $r = R_1$ (hollow sphere)

(ii) $\dfrac{\partial [W]}{\partial x} = 0$ at $x = 0$ (film)

or

$$\frac{\partial [W]}{\partial r} = 0 \text{ at } r = 0 \text{ (solid sphere) or } r = R_2 \text{ (hollow sphere)} \qquad 5(b)$$

where $[P_1]_0$ is the molar concentration of the pure monomer and $[W]_s$ is the interfacial concentration of the condensation product at the surface where the vacuum is applied. $[W]_s$ will be related to the partial pressure of W in the gas phase through some thermodynamic equilibrium relationship as, for example, Henry's law. The boundary condition, eq. (5b) (ii), is to account for the flux being zero at the metal wall in the case of the film or arises because of symmetry at $r = 0$ (solid sphere) or $r = R_2$ (hollow sphere).

The average value of the concentration of any species, for example P_i, is obtained by an appropriate spatial integration as

$$\begin{aligned} [P_i]_{av} &= \frac{1}{L}\int_0^L [P_i]\,dx && \text{(film)} \\ &= \frac{3}{R_2^3}\int_0^{R_2} [P_i] r^2\,dr && \text{(solid sphere)} \\ &= \frac{3}{R_2^3 - R_1^3}\int_{R_1}^{R_2} [P_i] r^2\,dr && \text{(hollow sphere)} \end{aligned} \qquad (6)$$

The number- and weight- average chain lengths are defined by

$$\mu_n = \frac{\sum_{n=1}^{\infty} n[P_n]}{\sum_{n=1}^{\infty} [P_n]} \qquad \mu_w = \frac{\sum_{1}^{\infty} n^2[P_n]}{\sum_{1}^{\infty} n[P_n]} \qquad (7)$$

with the polydispersity index ρ being the ratio of μ_w and μ_n. The spatial average number- and weight-average chain lengths and polydispersity index, $\bar{\mu}_n$, $\bar{\mu}_w$, and $\bar{\rho}$, can be obtained from eq. (7) by using average concentrations in place of local values.

The above equations are nondimensionalized using the following variables[10,24]:

$$X = k_p [P_1]_0 t$$

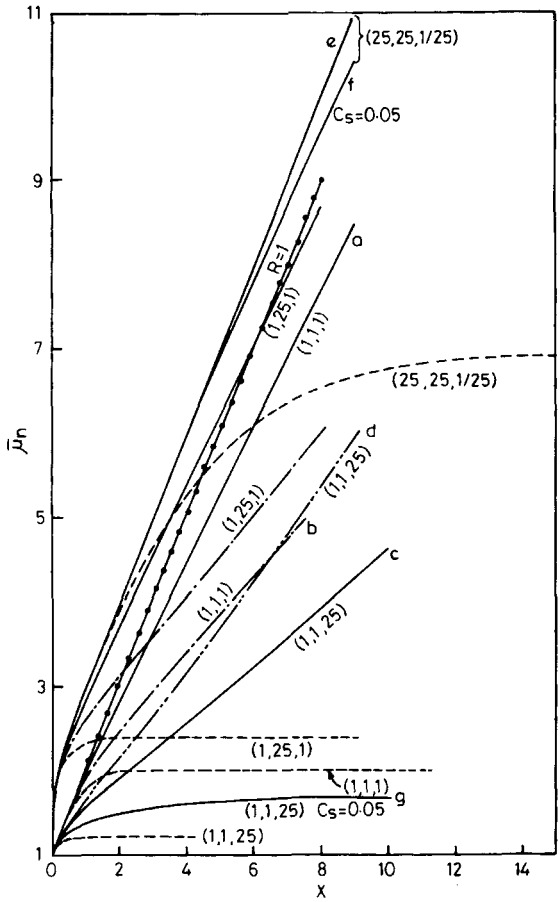

Fig. 2. Plot of $\bar{\mu}_n$ vs. X for various rate parameters indicated as (K_{eq}, R, R') for a small solid sphere, $\xi_2 = 2$ (—), large solid sphere, $\xi_2 = 4$ (— - —), and hollow sphere, $\xi_1 \simeq 2$, $\xi_2 \simeq 2.52$ (— - - —). Corresponding curves for no-mass transfer (- - -) and irreversible reactions (—·—·—) are also shown. Curve for irreversible case for $R = 25$ is almost identical to that for small solid sphere for $K_{eq} = 25$, $R = 25$, $R' = 1/25$, $C_s = 0$; C_s is zero except where indicated otherwise.

$$
\begin{aligned}
Z_i &= [\mathrm{P}_i]/[\mathrm{P}_1]_0 \qquad i = 1, 2, \ldots \\
C &= [\mathrm{W}]/[\mathrm{P}_1]_0 \\
R &= k_{11}/k_p \\
K_{eq} &= k_p/k_p' \\
R' &= k_e'/k_p' \\
\xi &= \sqrt{k_p[\mathrm{P}_1]_0/D_w}\,\zeta \\
\xi_1 &= R_1\sqrt{k_p[\mathrm{P}_1]_0/D_w} \\
\xi_2 &= R_2\sqrt{k_p[\mathrm{P}_1]_0/D_w} \text{ or } L\sqrt{k_p[\mathrm{P}_1]_0/D_w}
\end{aligned}
\tag{8}
$$

and are solved numerically.

The finite difference technique[33] is applied to these equations to obtain expressions for the (dimensionless) concentration of any species at any location

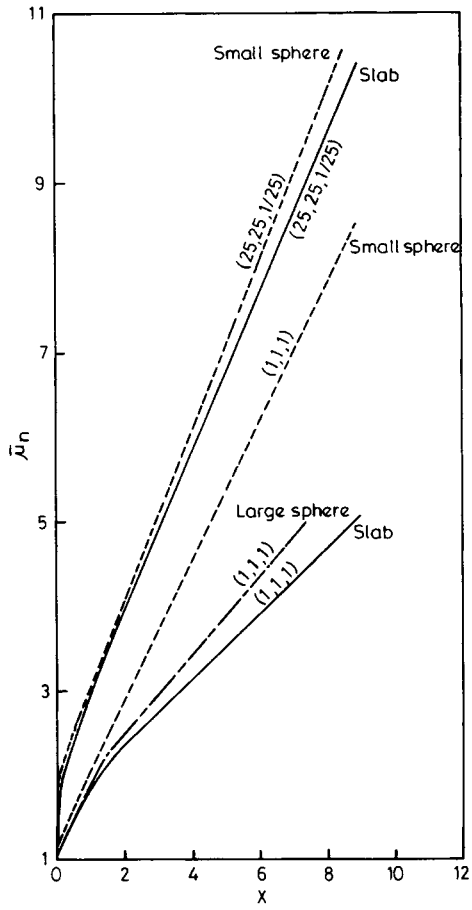

Fig. 3. $\bar{\mu}_n$ vs. X for two sets of rate parameters for an infinite slab: $\xi_2 = 2$, $C_s = 0$. Results for small solid sphere (- - -) and large solid sphere (— - —) shown for comparison.

at (dimensionless) time $(k + 1)\,\Delta X$ in terms of the various concentrations at time $k(\Delta X)$. L' Hopital's rule along with symmetry conditions are used to take care of the boundary condition in eq. (5b) (ii) for the film and solid sphere models, while for the hollow sphere the symmetry condition suffices.

For assuring proper convergence of the numerical procedure, the coefficient of ${}^{k}C_j$ (the value of C at the jth location and kth time interval) in the final equation for ${}^{k+1}C_j$ must be either positive or zero. This gives

$$\frac{(\Delta\xi)^2}{(\Delta X)} \geq 2 + \lambda \frac{\Delta\xi}{\xi} \tag{9}$$

Since the maximum value of $(\Delta\xi)/\xi$ is unity, one can use the following relationship between the increments of X and ξ for convergence:

$$(\Delta\xi)^2 = (2 + \lambda)\Delta X \tag{10}$$

The finite-difference equations so obtained were solved on a DEC 1090 computer to obtain the MWD and its moments as a function of time and location, for several values of the parameters R, K_{eq}, R', ξ_1, and ξ_2. The spatial-average MWD and

TABLE I
Spatial Variation of [W], μ_n, and ρ for the Small, Solid Sphere

Location	$C_s = 0$ (25, 25, 1/25), $\bar{X} = 14.1$, $\bar{p} = 0.9374$			$C_s = 0.05$ (1, 1, 25), $\bar{X} = 10$, $\bar{p} = 0.4038$		
j	C	μ_n	ρ	C	μ_n	ρ
0	0.0025	15.8235	1.8688	0.0520	1.6521	1.7319
1	0.0025	15.8262	1.8688	0.0520	1.6526	1.7329
2	0.0024	15.8362	1.8690	0.0519	1.6538	1.7349
3	0.0023	15.844	1.8692	0.0518	1.6560	1.7385
4	0.0021	15.8606	1.8695	0.0516	1.6591	1.7438
5	0.0019	15.8824	1.8699	0.0514	1.6632	1.7507
6	0.0016	15.9095	1.8704	0.0511	1.6680	1.7592
7	0.0013	15.9417	1.8711	0.0508	1.6735	1.7691
8	0.0009	15.9788	1.8718	0.0505	1.6794	1.7803
9	0.0005	15.0208	1.8726	0.0503	1.6857	1.7925
10	0.0000	16.0675	1.8735	0.0500	1.6919	1.8055
Average	0.0010	15.8695	1.8709	0.0507	1.6772	1.7771

its moments were also computed at different times. A typical run for one set of parameter values took approximately 130 min of computer time for X up to about 15. The value of $\Delta\xi$ was chosen independently so as to give the number of grid points as 11, and the corresponding value of ΔX was computed using eq. (10). A halving of the value of $\Delta\xi$ did not lead to any significant change in the computed results for equal values of X. Another check on the program was to obtain $\Sigma_1^\infty n Z_n$ from the computed values of Z_n at each location after every time interval. These matched with the theoretically expected value of unity to within 0.01% in the longest run when X went to 15. It may be added that this has been found to be an extremely sensitive check on the computer program in our earlier studies[10,23,27,28,30,31] on various polymerizations. Also, Flory's most probable distributions were obtained when C was put equal to zero at all locations and times. These checks confirmed that the computer program was free of errors.

Due to the reversible nature of the polymerization, the mass balance equation for any species P_n contains the concentrations of the higher species P_{n+i}, $i = 1, 2, \ldots$. Because of this fact, these equations cannot be solved sequentially (along with an equation for [P]) as is usually done for irreversible polymerizations, and some cut-off in the number of equations to be solved simultaneously is necessary. The method used in this study started with a total of 50 equations for P_n (i.e., equations for $P_1, P_2, \ldots P_{50}$), and the concentrations of all the higher oligomers were assumed to be zero. As soon as the dimensionless spatial average concentration of P_{50} increased to 10^{-10}, 10 more equations for P_n were added to each location. In other words, how the equations for $P_1, P_2, \ldots P_{60}$ were solved simultaneously, with the concentrations of P_{61}, etc., being put equal to zero. This procedure of adding on 10 more equations to the computational scheme was repeated every time the dimensionless average concentration of the last species went above 10^{-10}. Such a procedure has been found satisfactory in some of our previous simulations of reversible polycondensations but does not guarantee good results since there is at least one system, viz., nylon 6,[27,28] wherein an alternate procedure of adding on equations had to be used to obtain reasonable results, involving considerable man–machine interaction.

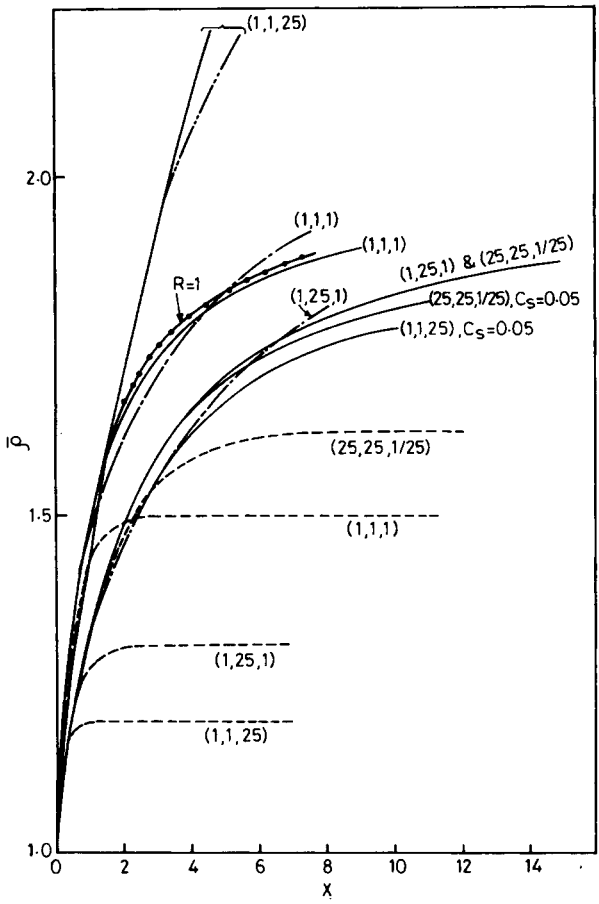

Fig. 4. $\bar{\rho}$ vs. X for the same systems as in Fig. 2. Notation same as in Fig. 2.

RESULTS AND DISCUSSION

Several simulations were carried out in order to study quantitatively the effects of various parameters on the MWD and its moments. The rate parameters were varied from the set of values $K_{eq} = 1, R = 1, R' = 25$, wherein the reverse reactions are slightly favored due to R' being larger than unity, to the other extreme $K_{eq} = 25, R = 25, R' = 1/25$, where the forward reactions dominate. The following reactor parameters were studied: two sizes of solid spheres, the small sphere having dimensionless radius $\xi_2 = 2$ and the large sphere having $\xi_2 = 4$, a hollow sphere having inner diameter $\xi_1 = 2$ and outer diameter $\xi_2 = 2.52$ (so that it has the same mass and the same inner surface area as the small sphere), and an infinite slab having $\xi_2 = 2$ (so that it has the same thickness as the radius of the small sphere). The solid sphere having $\xi_2 = 2$ corresponds physically to a sphere approximately 7.5×10^{-3} to 0.28 cm in diameter if typical values[25,26] of $D_W = 10^{-5}$ cm^2/s, $k_p = 150$ to 0.1 cm^3/mol-s, and $[P_1]_0 = 0.005$ mol/cm^3 are used. Similarly, the hollow sphere studied physically corresponds to spherical vapor bubbles of diameter 7.5×10^{-3} cm (or 0.28 cm for $k_p = 0.1$) with a center-to-center separation of about 18.9×10^{-3} cm (0.71 cm). The surface concentration of the condensation product was assumed zero in most cases except one, where

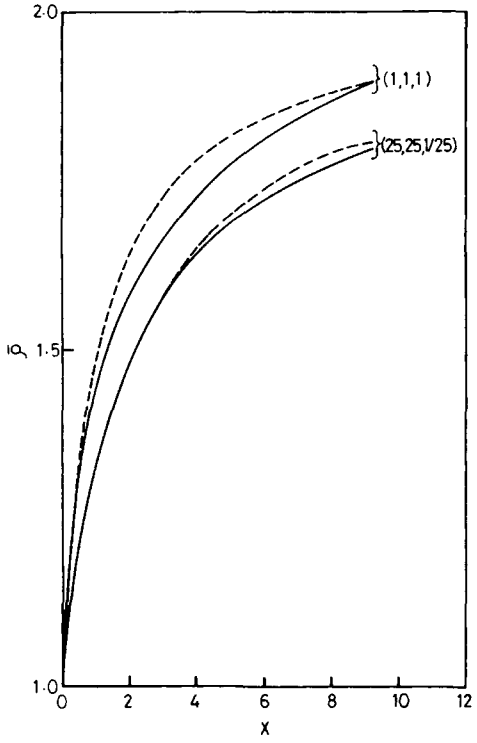

Fig. 5. $\bar{\rho}$ vs. X for an infinite slab. Notation as in Fig. 3.

the dimensionless value C_s was taken as 0.05, corresponding to $[W]_s$ of approximately 0.00025 mol/cm^3. Typical values for polyester reactors[26,31] lie between these values at about 10^{-6} mol/cm^3, corresponding to pressures of about 1–10 Torr.

Figures 2 and 3 show plots of the spatial average value of the number-average chain length $\bar{\mu}_n$ vs. the dimensionless time X, for various conditions. A comparison of the curves for any value of K_{eq}, R, and R' with the corresponding dotted curves in Figure 2 shows that substantially higher values of $\bar{\mu}_n$ are obtained in *all* reactor geometries when the condensation product is removed continuously by application of a vacuum and the reactions thus driven in the forward direction. It is found (e.g., curves a and b, Fig. 2) that for the same surface concentration of W, the large solid sphere gives lower values of $\bar{\mu}_n$ than the small sphere because the resistance to mass transfer is higher in the former and rates of diffusion of W are smaller. Similarly, from Figure 3, it is observed that a sphere which has relatively higher surface area gives larger $\bar{\mu}_n$ than an infinite slab having the same thickness. The values of $\bar{\mu}_n$ for the hollow sphere (curves c and d in Fig. 2), however, which has the same surface-to-volume ratio as the small solid sphere but is much thinner and so offers lower resistance to mass transfer, are higher than for the solid sphere. This emphasizes that in polycondensation reactors, the total surface area available for mass transfer per unit mass of the polymerizing liquid as well as the geometry are both extremely important variables.

These effects are less important when the rate parameters are such that the

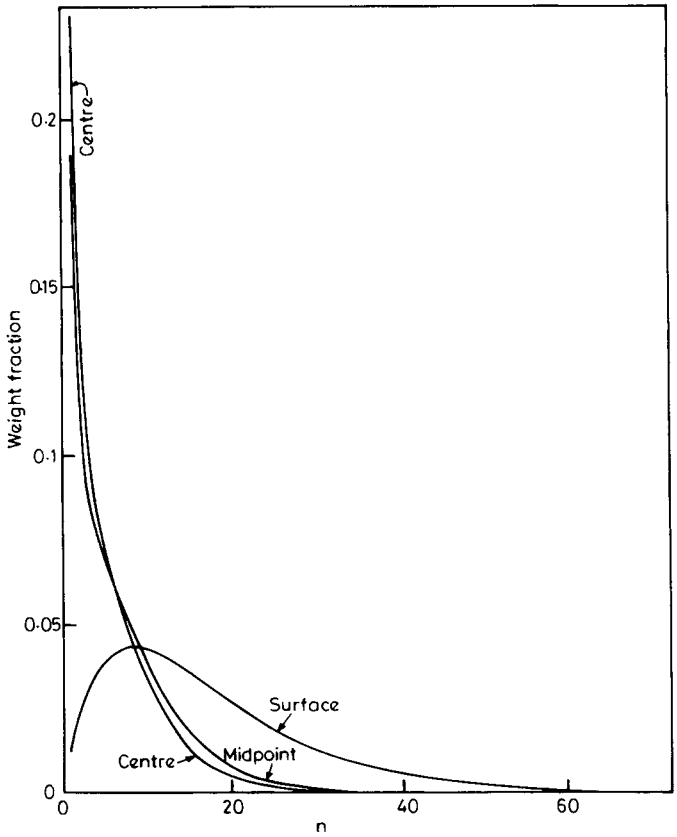

Fig. 6. MWD for $K_{eq} = 1, R = 1, R' = 25, C_s = 0, X = 8$ for the small, solid sphere at the center, midpoint, and surface.

reactions are almost irreversible, e.g., when $K_{eq} = 25$, $R = 25$, $R' = 1/25$. The effect of varying the surface concentration of W (i.e., the degree of vacuum) is also seen to be relatively small when the reactions are almost irreversible (e and f, Fig. 2) but is significant when the reverse reactions are important (c and g, Fig. 2). The influence of the rate parameters with other variables constant can be observed from the study of the results on the small solid sphere. The values of $\bar{\mu}_n$ are highest when the rate parameters favor the forward reaction (e, Fig. 2), e.g., for $K_{eq} = 25$, $R = 25$, and $R' = 1/25$, and are lowest (c, Fig. 2) when $K_{eq} = 1$, $R = 1$, and $R' = 25$. Thus, it is observed that the effect of mass transfer is to shift the $\bar{\mu}_n$ vs. X curves from the reversible, no-mass transfer curves toward the corresponding curves for irreversible reactions characterized by the same R. The amount of this shift depends on the reactor geometry, surface concentration of W, and the rate parameters.

It may be emphasized that $K_{eq} = R = R' = 1$ represents the equal reactivity case (studied by earlier workers[22,24,26]) for the same initial conditions as used in this work. The effect of the unequal reactivity of functional groups can thus be observed by comparing the other graphs with those marked(1, 1, 1).

Table I illustrates the spatial variation of [W], μ_n, and ρ at large values of X for two sets of conditions. Though the variation of [W] is appreciable, not too

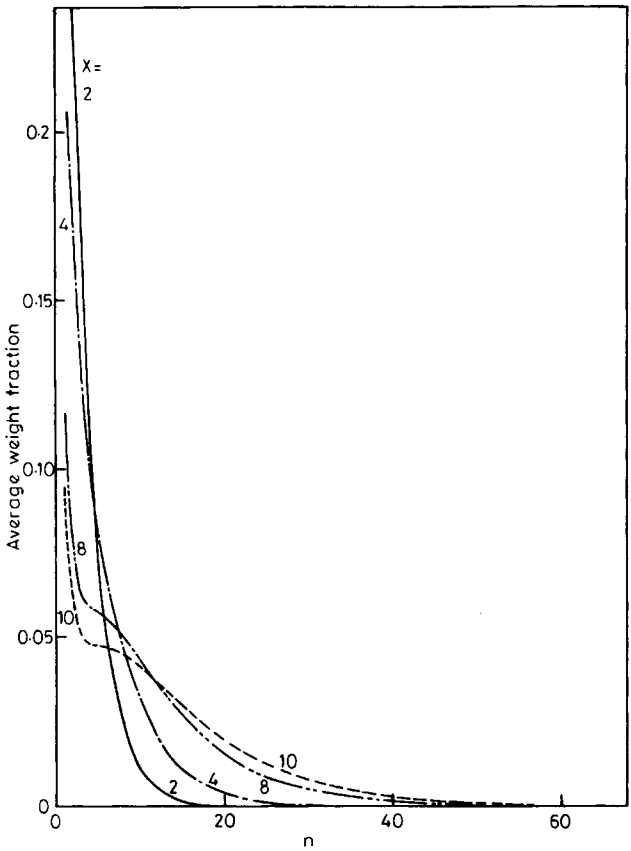

Fig. 7. Average MWD for $K_{eq} = 1, R = 1, R' = 25, C_s = 0$ for the small solid sphere at various X. Weight fraction monomer for $X = 2$ is 0.3191.

much variation is observed for μ_n and ρ. A similar observation of μ_n not varying appreciably with position was made by Secor[24] for the equal reactivity case, starting from an equilibrium polymer.

The spatial-average polydispersity index $\bar{\rho}$ is shown as a function of the dimensionless time for the same conditions in Figures 4 and 5. The values of $\bar{\rho}$ are found to be much higher in the presence of mass transfer than in its absence. It is interesting to observe that for the case when the forward reactions are favored, $\bar{\rho}$ is lower, though the average chain length $\bar{\mu}_n$ is higher than when the reverse reactions are important. The results are found to be relatively insensitive to the reactor geometry or the extent of vacuum applied, except for one case where $K_{eq} = 1, R = 1$, and $R' = 25$.

The MWDs at different locations and their spatial averages in the presence of mass transfer have been obtained for the first time here. Earlier studies were limited to obtaining μ_n only, since they worked in terms of functional groups instead of with molecular species. The MWDs depend markedly on the location when the reverse reactions are important ($K_{eq} = R = 1, R' = 25$), as shown in Figure 6 for the small sphere. It is observed that for this case, there are substantial amounts of unreacted monomer in the inside region, though near the

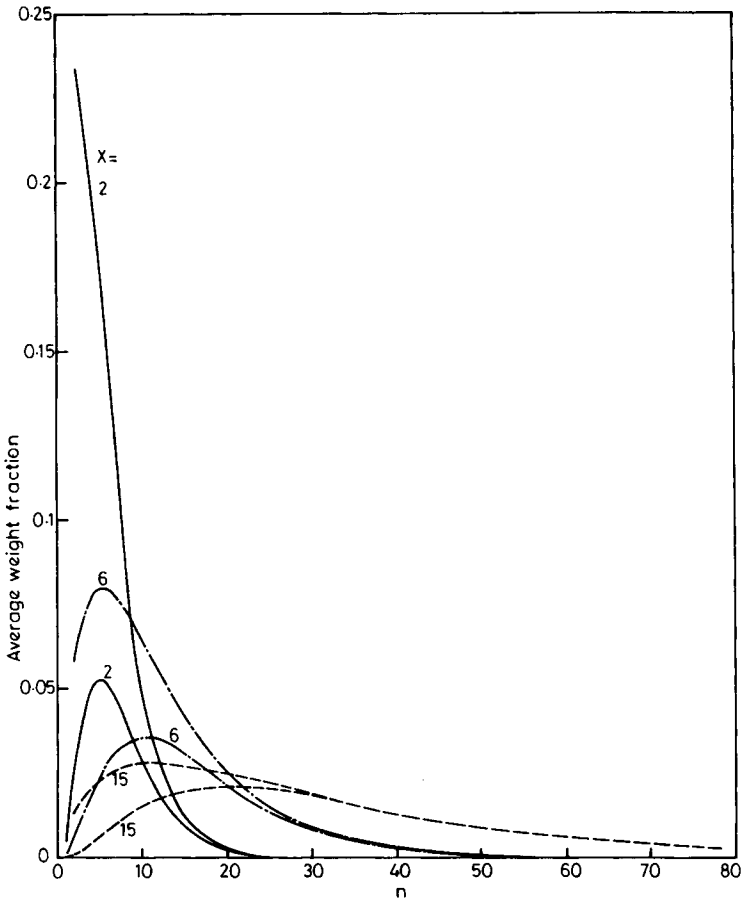

Fig. 8. MWD for $K_{eq} = 25$, $R = 25$, $R' = 1/25$, $C_s = 0$ for the small solid sphere for various X. Lower curve for any X is for odd values of n and upper curves for even n. Graphs corresponding to various locations are indistinguishable.

surface, the characteristic hump is seen. The spatial average MWD for the same system is shown in Figure 7 for different values of X. The characteristic shape of these curves at X around 10 is due to the preponderance of unreacted monomer at the center of the sphere, and a hump seems to be just appearing at higher times. When the forward reactions are rapid ($K_{eq} = R = 25$, $R' = 1/25$), there is very little difference between the MWDs at different locations, and the average MWDs are shown in Figure 8. It is observed, however, that the MWD curves split into two for such cases—one (lower) corresponding to odd values of n and one for even values. This split in the MWDs is characteristic of polymerizations characterized by unequal reactivity of functional groups for $R > 1$. The separation between the odd- and even-n curves decreases as X increases.

Figure 9 shows the spatial-average MWD for the small sphere in the presence of mass transfer when the average conversion of functional groups, $\bar{p}$, is 0.8515 (corresponding to $X = 4.8$). Corresponding results in the absence of mass transfer effects[10] for about the same conversion of functional groups, 0.8519 (corresponding to $X = 10$), are also shown for comparison. The split in the odd-

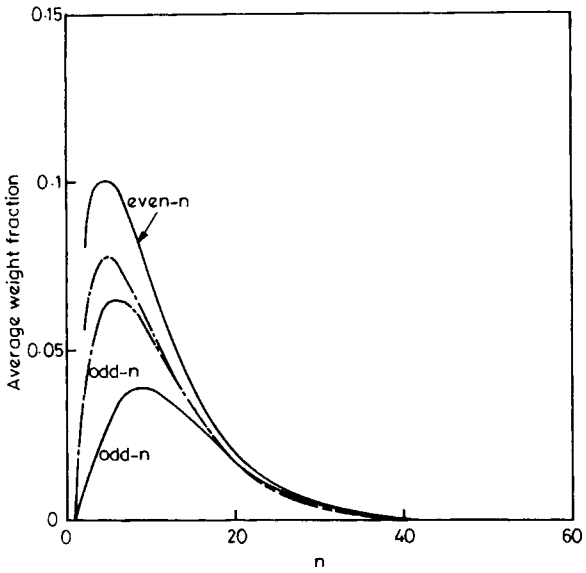

Fig. 9. Average MWD for the small sphere, (25, 25, 1/25) $C_s = 0$, $X = 4.8$ (solid lines). Results in the absence of mass transfer for the same functional group conversion shown by (— - - —). Results for irreversible case with $R = 25$ are very close to solid lines.

and even-n curves is found to be higher in the presence of mass transfer, which takes the system toward irreversibility.

The presence of mass transfer is thus observed to take the MWDs from the results obtained earlier in the absence of mass transfer[10] (sealed tube polymerization) toward the results for irreversible polymerizations for the same R.

References

1. P. J. Flory, *Principles of Polymer Chemistry*, Cornell University Press, Ithaca, NY, 1953.
2. S. K. Gupta and A. Kumar, *Chem. Eng. Commun.*, to appear.
3. A. Kumar and S. K. Gupta, *Fundamentals of Polymer Science and Engineering*, Tata McGraw-Hill, New Delhi, 1978.
4. W. H. Ray, *J. Macromol. Sci. C*, **8**, 1 (1972).
5. T. T. Szabo and J. F. Learthrum, *J. Appl. Polym. Sci.*, **13**, 561 (1969).
6. J. A. Biesenberger, *A.I.Ch.E.J.*, **11**, 369 (1965).
7. J. Hicks, A. Mohan, and W. H. Ray, *Can. J. Chem. Eng.*, **47**, 590 (1969).
8. N. H. Smith and G. A. Sather, *Chem. Eng. Sci.*, **20**, 15 (1965).
9. Z. Tadmore and J. A. Biesenberger, *Ind. Eng. Chem., Fundam.*, **5**, 336 (1966).
10. S. K. Gupta, P. Rajora, N. L. Agarwalla, and A. Kumar, *Polymer*, to appear.
11. R. Goel, S. K. Gupta, and A. Kumar, *Polymer*, **18**, 851 (1977).
12. S. K. Gupta, A. Kumar, and A. Bhargava, *Polymer*, **20**, 305 (1979).
13. S. K. Gupta, A. Kumar, and A. Bhargava, *Eur. Polym. J.*, **15**, 557 (1979).
14. K. S. Gandhi and S. V. Babu, *A.I.Ch.E.J.*, **25**, 266 (1979).
15. E. Ozizmer and G. Odian, *J. Polym. Sci. Polym. Chem. Ed.*, **18**, 1089 (1980).
16. D. R. Miller and C. W. Macosco, *Macromolecules*, **11**, 656 (1978).
17. S. K. Gupta, A. Kumar, and R. Saraf, *J. Appl. Polym. Sci.*, **25**, 1049 (1980).
18. A. Kumar, S. K. Gupta, and R. Saraf, *Polymer*, **21**, 1323 (1980).
19. K. Ravindranath and K. S. Gandhi, *Chem. Eng. Sci.*, **3**, 955 (1980).
20. A. SenGupta, A. Kumar, and S. K. Gupta, *Br. Polym. J.*, **13**, 76 (1981).
21. W. H. Abraham, *Chem. Eng. Sci.*, **21**, 327 (1966).
22. D. A. Mellichamp, *Chem. Eng. Sci.*, **24**, 125 (1969).

23. S. K. Gupta, N. L. Agarwalla, P. Rajora, and A. Kumar, *J. Polym. Sci. Polym. Phys. Ed.*, to appear.

24. R. M. Secor, *A.I.Ch.E.J.*, **15,** 861 (1969).

25. P. F. Hoftyzer and D. W. Van Krevelen, in *Proceedings of 4th European Symposium on Chemical Reaction Engineering*, Brussels, Sept. 9–11, 1968, Pergamon, New York, 1971, p. 139.

26. M. Amon and C. D. Denson, *Ind. Eng. Chem., Fundam.*, **19,** 415 (1980).

27. S. K. Gupta, A. Kumar, P. Tandon, and C. D. Naik, *Polymer*, **22,** 481 (1981).

28. S. K. Gupta, C. D. Naik, P. Tandon, and A. Kumar, *J. Appl. Polym. Sci.*, **26,** 2153 (1981).

29. A. Kumar, S. Kuruville, A. R. Raman, and S. K. Gupta, *Polymer*, **22,** 387 (1981).

30. A. Kumar, A. K. Kulshrestha, and S. K. Gupta, *Polymer*, **21,** 317 (1980).

31. A. Kumar, S. K. Gupta, B. Gupta, and D. Kunzru, *J. Appl. Polym. Sci.*, to appear.

32. V. Gupta and J. Srinivasan, *Heat and Mass Transfer*, Tata McGraw-Hill, New Delhi, 1978.

33. H. S. Mickley, T. K. Sherwood, and C. E. Reed, *Applied Mathematics in Chemical Engineering*, 2nd ed., McGraw-Hill, New York, 1957.

34. A. S. Foust, L. A. Wenzel, C. W. Clump, L. Maus, and L. B. Anderson, *Principles of Unit Operations*, 2nd ed., Wiley, New York, 1980.

Received May 1, 1981
Accepted August 25, 1981